

## 13

# The Use of Imagery in Laboratory Experiments

Michal Tal<sup>1</sup>, Philippe Frey<sup>2</sup>, Kim Wonsuck<sup>3</sup>, Eric Lajeunesse<sup>4</sup>, Angela Limare<sup>4</sup> and François Métivier<sup>1</sup>

<sup>1</sup>Aix-Marseille Univ CEREGE, UMR 6635, 13545 Aix-en-Provence Cedex 04,

<sup>2</sup>Irstea, F-38402 St-Martin-d'Hères, France

<sup>3</sup>The University of Texas at Austin, Texas 78758-4445, United States

<sup>4</sup>Institut de Physique du Globe de Paris, Sorbonne Paris Cité, Paris, France

## 13.1 Introduction

Experimental-based research in fluvial geomorphology constitutes an important tool for studying processes occurring in natural rivers. Laboratory experiments are useful for inspiring questions, testing hypotheses, and identifying key processes and parameters. Insights from studies using laboratory stream-tables (relatively wide shallow containers in which the experimental river sets its own width and pattern) and flumes (relatively long narrow channels with fixed parallel side walls) underlie our understanding of processes such as bedload transport (e.g., Gomez and Church, 1989), controls on channel width (e.g., Ikeda et al., 1988), downstream fining (e.g., Seal et al., 1997), and the mechanics of flow through bends (e.g., Hooke, 1975), and have led to important insights about the underlying physics of large and chaotic systems such as braided rivers and deltas (e.g., Ashmore, 1991b; Sapozhnikov and Fofoula-Georgiou, 1997, Kim and Paola, 2007; Hoyal and Sheets, 2009).

Laboratory experiments lend themselves well to studies that are relevant to stream restoration and management because they provide a relatively inexpensive, fast, and simple way to collect large quantities of data under controlled conditions. Full control means that variables

can be held fixed and the role of individual variables can be isolated. Experiments enable observation of long-term behaviour that can often only be predicted or inferred in the field. This is important because processes being studied in the field typically evolve well beyond the typical time frame of a grant or monitoring program and insight from long-term observation is often missed. Finally, the ability to collect data from an experiment using several different techniques permits researchers to draw conclusions based on an aggregate of measurements, while multiple runs allow for more rigorous statistics and greater confidence in results.

This chapter deals with the use of imagery to acquire data from laboratory experiments. Imagery in the laboratory provides the same advantages as in the field: data acquisition at very high temporal and spatial resolutions in an entirely non-invasive manner. Experiments have the intrinsic advantage offered by satellites and airplanes to study natural systems; a view of the system through a lens zoomed way out. Imaging techniques in the laboratory are enhanced by the high degree of control over lighting and materials which can both simplify image processing and greatly enhance the results. Despite these inherent advantages, the technology to collect information to the

### 300 Fluvial Remote Sensing for Science and Management

full potential an experiment can offer has only recently become readily available, mainly in the form of inexpensive digital cameras. Today it is common to conduct experiments in which imaging is the only method of data collection.

We present several imaging techniques that offer a broad range of applications related to river management (Table 13.1). These techniques are based on the use of cameras ranging from simple digital cameras and video recorders to more sophisticated CDD cameras and high-speed video recorders. The experiments presented were conducted in a wide range of flumes and stream tables and thus provide an idea of the diversity of setups and methods used in experimental geomorphology (Table 13.1). Our focus is on imagery techniques used in studies of river channels and deltas to measure (a) mass flux of sediment: sediment grainsize distribution, bedload transport rate, trajectories and velocities of individual particles, (b) local and regional properties of the flow field: depth, width, migration rates, sinuosity, braiding index, and (c) bed topography in river channels and deltas (Table 13.1). This chapter is not an exhaustive review of imagery techniques used in the laboratory. We concentrate on a few key examples which illustrate how the powerful combination of laboratory experiments and imagery can be used to advance our understanding of river processes and inform management. (Commercial software and brand names of equipment used in the studies presented here are included purely as examples based on the authors' experience. The methodologies described do not depend on any specific software packages or equipment and references to these do not constitute endorsement).

#### 13.2 Bedload transport

Fundamental to the study of the dynamics of any river is characterising the rate (mass or volume per unit time) of sediment transported as bedload and the size distribution of the transported material. In addition, detailed data about bedload transport at the grainscale under different flow conditions are needed in order to improve our understanding of the physics governing bedload transport and derive physically based transport equations and models. However, direct measurements of bedload transport in rivers are difficult and can be dangerous during larger flows, which account for most of the sediment flux (Wilcock, 2001). In addition, direct measurements



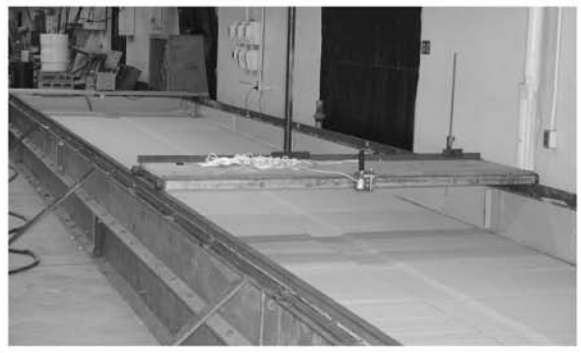

yield imprecise estimates due to the inherent spatial and temporal variability in the processes of bedload transport (Diplas et al., 2008). Flume experiments have been used extensively to improve our understanding of sediment transport processes (e.g., Parker et al., 1982) and many of the most widely used bedload transport equations were derived from experimental data (e.g., Meyer-Peter and Muller, 1948; Wilcock and Crowe, 2003). Experimentally, measuring bedload transport rate and obtaining a grain-size distribution (GSD) of the material transported (in the case of non-uniform bed mixtures) typically consists of collecting the sediment at the flume outlet, manually sieving the sample, and weighing the individual size fractions. Needless to say, this is a cumbersome and time-consuming task.

Even more difficult to measure than sediment transport in the field is bed surface size distribution, which directly affects the observed transport (Wilcock, 2001). As in the case of sediment transport, the bed surface in natural rivers can often be sampled under low flow conditions, but is almost impossible to sample during high transport conditions. Several methods for automated grainsize estimation from images exist (Rubin, 2004; Graham et al., 2005; Buscombe et al., 2009, 2010). These techniques were developed for field applications but can be adapted to laboratory experiments. Because flow in a flume can be instantaneously shut off, experiments offer a unique opportunity to study the bed surface associated with active transport. This makes flume experiments particularly useful for addressing questions such as what happens to surface armour layers during high flow and improving our understanding of fractional transport. In a well-known set of experiments conducted in the 'bed of many colours' (BOMC), imagery was used in an innovative way to estimate bed surface grainsize distribution (and from this variations in grain mobility) during active transport in a way that was non-destructive to the bed (details in Wilcock and McARDell, 1993; Wilcock, 2001). In these experiments each size fraction in the sediment bed was painted a different colour. Photographs of the bed surface when the flow was turned off were used to measure the grainsize distribution using point counts.

Here we present two techniques for studying sediment transport dynamics in experimental channels. The first is an image-based technique which enables continuous in-line measurement of size and velocity of all transported particles at the downstream exit of a flume. This information is then used to determine the GSD and total sediment discharge. The second technique uses imagery to reconstruct 2D trajectories of individual grains

13 The Use of Imagery in Laboratory Experiments 301

**Table 13.1** Examples of experimental facilities used to study rivers and deltas. W, L, and D are the width, length, and depth respectively.

	<p>Flume with adjustable width and slope typically used for experiments to study sediment transport. W = 0.096 m, L = 0.24 m, IPGP experimental geomorphology laboratory.</p>
	<p>Stream table with adjustable slope typically used for experiments to study channel morphodynamics, IPGP experimental geomorphology laboratory. W = 0.75 m L = 2 m</p>
	<p>Large stream table with fixed sidewalls typically used for experiments on channel morphology and interactions with riparian vegetation, St. Anthony Falls Laboratory. W = 2 m L = 16 m</p>
	<p>Experimental tank with subsiding floor designed to study the links between deltaic processes, subsidence, and base level, St. Anthony Falls Laboratory. W = 3 m L = 6 m D = 1.5 m</p>

### 302 Fluvial Remote Sensing for Science and Management

transported as bedload. This technique applies particle tracking velocimetry (PTV) algorithms commonly used in studies of fluid mechanics and, more recently, suspended sediment in flows.

#### 13.2.1 Image-based technique to measure grainsize distribution and sediment discharge

The objective of the technique presented here is to characterise GSD by weight and total sediment discharge exiting the downstream end of a flume. The methodology is based on image analysis of sediment in the sand and gravel size range flowing across a light table (Frey et al., 2003; Figure 1). The equipment required for this technique are a light table that can be tilted independently of the flume (in the study described here, this consisted of an adjustable transparent ramp with a light source fixed underneath it) and a digital video recorder that can operate in backlighting mode. The aim is to have particles move across the table in a single layer with a low number of clusters and the thinnest possible flow. The tilt of the table should be adjusted to obtain the smoothest possible flow and dispersion of particles. For a given sediment concentration exiting a flume, the steeper the ramp the higher the velocity will be and the lower the number of clusters. In the experiments described here, the velocity of sediment moving across the ramp was typically 2–6 m/s. A camera that captured full-frame monochrome images with a resolution of  $640 \times 480$  pixels and a frequency of 60 Hz was used (Bigillon et al., 1999). The range of medium diameters of the particles was initially restricted to about one order of magnitude, typically 2–20 mm, however the technique can be used to measure a larger grainsize

distribution by capturing images at higher frequency or using two cameras with different fields of view.

Assuming all the particles have the same density ( $\rho$ ), the mass of each particle is calculated from its volume ( $V$ ). Particles are described by their three principal dimensions: minimum diameter (the thickness), medium diameter ( $d$ ), and the maximum diameter ( $D$ ); the grain-size of each particle is characterised by the medium diameter ( $d$ ). If ( $v$ ) is the streamwise velocity of the particle (in pixels per second) and ( $h$ ) the streamwise length of the image (in pixels) the total sediment discharge is the sum of the elementary contribution of each particle :

$$Q_s = \sum_{i \in \text{particles}} \frac{\rho \cdot V(i) \cdot v(i)}{h} \quad (13.1)$$

where  $V(i)$  is the volume of the  $i$ th particle. This sum is calculated on all particles for all images. The GSD is derived from the sum of elementary sediment discharges relative to one class of medium diameters divided by the total sediment discharge. If all particles have the same constant streamwise velocity on the backlit plate, the problem is simplified to the ratios of the volumes of particles of one class of medium diameters to the total volume, i.e.:

$$\frac{\sum_{i \in \text{class}} V(i)}{V_{\text{tot}}} \quad (13.2)$$

In this case, streamwise velocity needs to be assessed in order to calculate total sediment discharge.

Calculating the volume of each particle is central to this methodology. To do this, image processing algorithms are first used to estimate the diameters and areas of the particles in the 2D image. Next, the volume is calculated

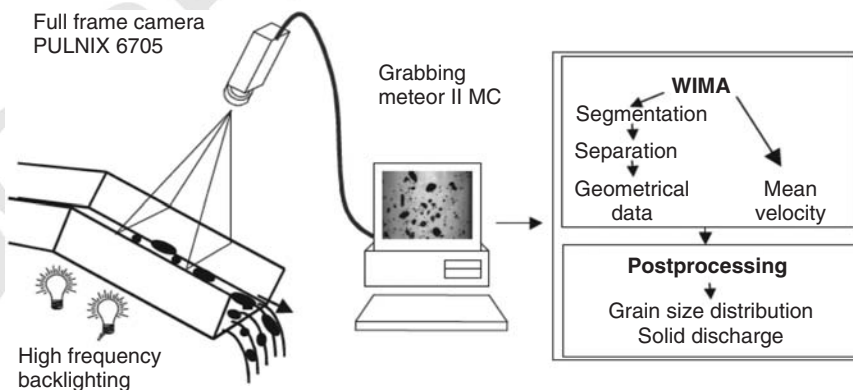


**Figure 13.1** Experimental setup and processing chain to characterise the grainsize distribution and sediment discharge exiting the downstream end of a flume using image analysis of sediment flowing across a light table.

## 13 The Use of Imagery in Laboratory Experiments 303

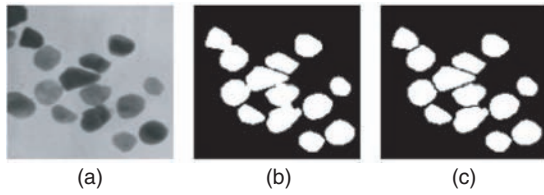


**Figure 13.2** Sequence of image processing steps for segmenting particles (a) original image (b) result after segmentation (c) result after object separation.

by assessing the third dimension perpendicular to the image plane. In the study presented here a user-friendly image processing software called WIMA, developed by the Laboratoire Huber Curien (formerly TSI) of the University of St. Etienne, was used (Ducottet, 1994). Any image processing software with standard functions and which permits users to modify and add new functions can be used. The main goal of the image processing algorithms is to segment the particles in order to gain access to their dimensions. The three main image-processing steps required to achieve this goal are segmentation (i.e., detection), object separation, and object measurement (Figure 13.2). Edge detection techniques based on the use of Canny gradient operators and localisation of maximum gradient modulus were used (Jernot et al., 1982; Canny, 1986). Once these steps are achieved, the final step in the image analysis consists of extracting the boundaries of all detected particles in the image series. It is then possible to calculate areas as well as minimum and maximum principal diameters.

Assessing the volume of each particle is rather difficult for particles with variable shapes, and several assumptions have to be made in order to do this. First, it must be assumed that the particles flow in their stable state. Considering that particles are described by their three principal dimensions, it is possible to measure the medium ( $d$ ) and maximum ( $D$ ) dimensions (corresponding to the minimum and maximum diameters in the image respectively) as well as area ( $A$ ) in the image plane. An ellipsoid shape is assumed for the particles, and thus grain thickness, which is perpendicular to the image plane, is a fraction of the medium diameter and is calculated using a shape coefficient ( $\alpha$ ). The shape coefficient ( $\alpha$ ) must be calibrated for the sediment being used. The volume of each particle then goes as:

$$V = \frac{\pi}{6} a \cdot d^2 D = \frac{2}{3} a \cdot d \cdot A \quad (13.3)$$

Preliminary tests showed that calculating the volume using area rather than diameters yielded more accurate

results (Frey et al., 2003). Since GSD is derived from the ratios of volumes, if the dispersion around the mean value of the shape coefficient ( $\alpha$ ) for each class of diameters is small it is not necessary to know this value. On the other hand, the sediment discharge cannot be computed without assessing at least the mean shape coefficient. It was thought initially that velocities of particles could be highly dispersed across the light table. However, preliminary tests showed that dispersion around the mean velocity was low. Furthermore, velocity was not correlated with diameter of particles. Using sediment with grainsizes ranging from 2–12 mm, the velocity of one class of diameters was found to deviate no more than 10% from the mean velocity, which is then only required to compute sediment discharge. Because calculating sediment discharge requires both mean streamwise velocity and at least a mean shape coefficient, estimates of sediment discharge are less accurate than estimates of the GSD.

Numerous tests were carried out in order to compare medium diameters and masses obtained by image analysis with measured values (see Frey et al., 2003). Motionless particles with known shape coefficients were tested in a first series. Diameters and mass predictions were good, with uncertainties on the order of 3% and 6% respectively. In a second series, the light table was attached to the outlet of an experimental flume. The flume was 15 cm wide and had the same width as the transparent ramp. A sample of 400 particles were mixed into the flow slightly upstream of the outlet in order to simulate real experimental conditions. Results were improved when volume calculations considered differentiated shape coefficients, although results were remarkably good even when a uniform shape coefficient was used. Considering the diameters commonly used to describe grainsize:  $d_{30}$ ,  $d_{50}$ , and  $d_{90}$ , where  $d_{xx}$  is the diameter for which  $xx\%$  by weight of the sample is finer, the errors were 4%, 3% and 1% respectively. The minimum number of particles needed to achieve a significant statistical measurement – a proxy for the length of time over which measurements should be collected – for both GSD and sediment discharge was approximately 4,000 particles. With more than 2,500 particles the computed value was within 3% of the actual value and with more than 1,500 it was approximately 7%. A much lower number of particles ( $\sim 1000$ ) were required for low discharges in which coarser particles were dominant and the GSD was more uniform. Empirical testing is recommended in order to determine the optimal number of particles needed to achieve a good statistical fit. This method has been used successfully to investigate mechanisms responsible for bedload

### 304 Fluvial Remote Sensing for Science and Management

sheet production and migration (Recking et al., 2009). It has also been adapted and improved to study step-pools experimentally (see Zimmermann et al., 2008).

#### 13.2.2 Particle trajectories and velocities using PTV

Particle tracking velocimetry (PTV) and a closely related technique – particle imagery velocimetry (PIV) were developed and are widely used in the field of fluid mechanics (for a review see Adrian, 2005 and Chapter 16, this volume). The use of these image-based techniques to study sediment transport has been steadily expanding; they were first applied to studies of suspended sediment transport in turbulent flows and more recently to bedload transport. Tracking a single detected particle in a series of images is relatively easy and a number of authors have used image analysis to measure the trajectories of saltating and rolling particles (e.g., Niño et al., 1994; Hu and Hui, 1996; Lee et al., 2000; Ancey et al., 2002, Ancey et al., 2003). Tracking sediment flux is more complex and requires segmentation of all the particles in the image as a first step. Segmentation can be achieved by applying algorithms commonly used in PTV. Such algorithms were specifically developed to track tracers in a flow in regions where standard PIV algorithms based on cross-correlations were not well adapted because of large velocity gradients. These algorithms were then applied to tracking suspended sediments. Sechet and Le Guennec (1999) investigated the role of near wall turbulent structures. Nezu and Azuma (2004) building on a technique described by Okamoto et al. (1995) used PTV to characterise particle-laden free surface flows. Studies tracking coarse material are rare: Pilotti et al. (1997) analysed incipient motion of dark coloured grains on a light coloured smooth bed, Papanicolaou et al. (1999) tracked green glass beads over a layer of fixed transparent ones. In both cases the number of particles being tracked was low and the contrast between the grains and the bed was sufficiently high to allow segmentation using simple colour thresholding procedures. In these studies only the motion of segmented particles was tracked, rather than the entire bed. In a more sophisticated application, Capart et al. (1997) investigated water-sediment interaction following a dam-break, in which segmentation was used to track the motion of 6 mm plastic beads. More recently, Spinewine et al. (2003) extended the work of Capart et al. (2002) to the study of granular flows.

We present two flume studies that use PTV to reconstruct 2D trajectories of grains transported as bedload. In the first study, images of a 2D bed captured in plan-view

were used to characterise the trajectories of bedload particles entrained by turbulent flow in a channel that was wide compared to the grainsize (Lajeunesse et al., 2010). In a second study, a high-speed camera was used to film the movement of particles flowing down a steep narrow channel only slightly wider than the grain diameter. In this study the 2D trajectories of the particles were captured in side-view of a transparent flume (Böhm et al., 2006).

##### 13.2.2.1 2D trajectories in plan-view of individual grains transported as bedload

The goal of the study presented here was to investigate the motion of bedload particles over a flat bed of uniform grainsize under steady, spatially uniform, turbulent flow. The methodology consists of capturing images in plan-view of bedload particles moving across a bed using a high-speed camera mounted directly above the flume. From image analysis, particle velocities, step (or flight) lengths and durations, and the surface-density of moving particles can be measured (vertical velocity and saltation height cannot be measured in plan-view). Details of the study and the methodology can be found in Lajeunesse et al. (2010).

The experiments were carried out in a rectangular tilting flume with a width of 0.096 m and length 0.24 m. Water was injected by a pump at the upstream inlet of the flume and flowed over a sediment bed composed of quartz grains several centimeters thick. Three series of experiments were performed with a  $D_{50}$  of 1.92, 2.6 and 5.5 mm respectively. No additional sediment was fed at the upstream and as a result an erosion wave slowly propagated from the inlet towards the outlet of the flume. All the experiments were stopped well before the erosion wave reached the study reach situated in the middle of the flume and therefore it did not influence the results (this was also verified by measurements of the bed slope at the start and end of the experiment which showed that it remained constant). Approximately 10% of the sediment particles in the bed were dyed black. The rest were the natural colour of quartz (i.e., clear to white). A high-speed camera (250 frames per second,  $1024 \times 1024$  pixels) mounted vertically directly above the bed was used to track the motion of the sediment particles. The position of the black particles could be tracked between successive frames with an interval of 0.04 s and the goal was to determine velocities and trajectories of each dyed bead from the temporal sequence of images (Figure 13.3). The spatial resolution of the camera was such that the particle diameter was about 50 pixels and the

13 The Use of Imagery in Laboratory Experiments 305

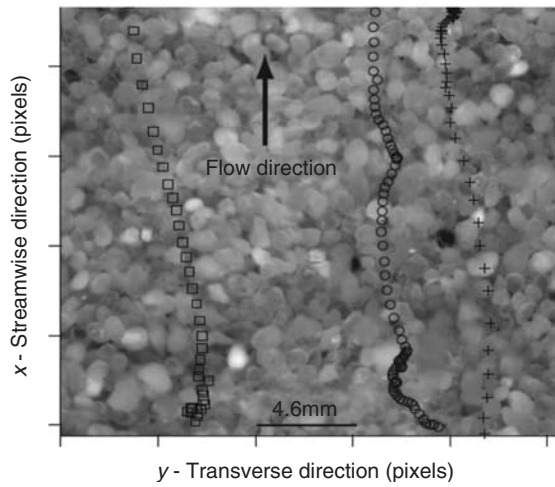


**Figure 13.3** Example of three particles trajectories determined using particle tracking algorithms. The time interval between two successive positions is 0.004 s. The field of view is  $23.5 \times 23.5 \text{ mm}^2$  (particle diameter is approximately 50 pixels).

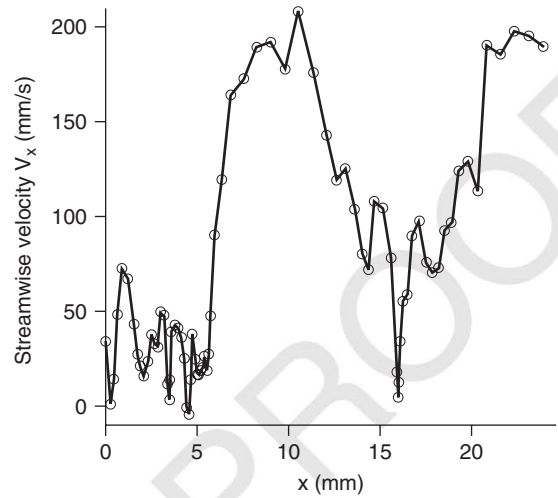


**Figure 13.4** Streamwise velocity of a single particle through time as it moves downstream.

field of view approximately  $20 \times 20$  particle diameters. At these conditions, the position of a dyed particle could be determined with an accuracy of 0.05 mm. Particle tracking was performed using algorithms developed using the IgorPro data processing software (Lajeunesse et al., 2010). The algorithm consisted of two steps. In the first step each image was thresholded and binarised to create an image in which the dyed particle was black and the particles that not dyed were white. A particle detection algorithm was applied in order to detect and localise the center of each black particle. Lighting quality and the choice of threshold criteria are crucial for this first step. The second step consisted of reconstructing particle trajectories by tracking the black beads through the sequence of images (Figure 13.3). The data were then processed to calculate streamwise and transverse particle velocities and their distributions (Figures 13.4 and 13.5).

The main source of error in the experiments performed by Lajeunesse et al. (2010) was oscillation of the water surface which caused an apparent movement of the particles. This error can be corrected by determining the apparent velocity of a particle at rest for each experiment. Based on measurements of apparent velocity, a threshold value is defined below which particle velocities are discarded. Lajeunesse et al. (2010) had threshold values between 10–30 mm/s, depending on the flow rate. The same particle-tracking algorithm can be used to compute lengths and durations of particle step-lengths. To do

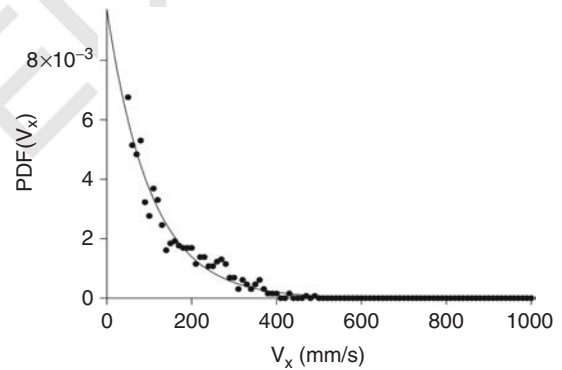


**Figure 13.5** Distribution of particle streamwise velocities ( $V_x$ ) measured using particle tracking algorithms. The PDFs decrease monotonically to zero and follow an exponential function.

this, the size of the field of view had to be increased so that it is sufficiently larger than the characteristic particle step-lengths.

13.2.2.2 Tracking of beads entrained in a quasi two-dimensional channel

In this study PTV was performed from the side of a quasi-two dimensional tilting flume (2 m long and 0.2 m high) with transparent walls. The width of the flume was only slightly wider than the width of the particle diameters (6.5 mm). The goal of the experiments was to study the motion of coarse spherical glass beads entrained by a

### 306 Fluvial Remote Sensing for Science and Management

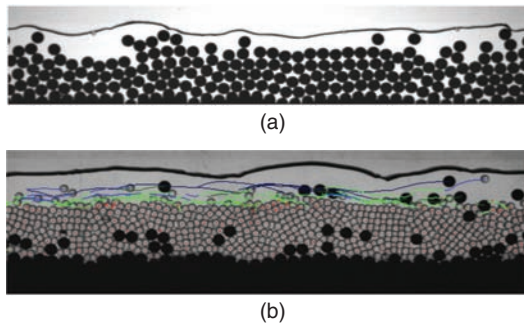


**Figure 13.6** (a) Image of a unimodal experiment with 6 mm beads, (b) image from an experiment with a two-size mixture, bead-trajectories corresponding to the previous 30 images are superimposed.

turbulent supercritical flow down a steep channel (slopes were between 7.5–15%). Details can be found in Böhm et al. (2004, 2006). The experiments were performed with one-size and two-size sediment mixtures (Figures 13.6a and 6b respectively). The channel was supplied continuously with beads and measurements were made when transport was at equilibrium over the mobile bed (Böhm et al., 2004). Image processing was used to determine velocities and trajectories of each bead from a temporal sequence of approximately 8,000 images (Böhm et al., 2006). Numerous measurements permitted a thorough statistical description of unimodal sediment transport based on stochastic Markov-type processes (Ancey et al., 2006, 2008).

As in the previous studies, image processing consisted of first detecting and localising all beads and then reconstructing their trajectories by tracking them through the sequence of images. Here again, the image processing software WIMA in combination with several custom designed algorithms was used. In this study all the particles present in the measurement window were tracked (as opposed to only coloured particles in the previous study) making segmentation a crucial step. The quality of segmentation is largely dependent on flume setup, lighting, and material, and requires blending of know-how on image acquisition and knowledge of segmentation algorithms. As a general rule, particle tracking works best when applied to high quality well-contrasted images achieved through the right combination of lighting and material. Experiments should be setup with PTV needs in mind; bad quality images result in numerous false detections and can hamper the possibility to perform tracking at all. In the uniform size experiment (Böhm et al., 2006), using a two-dimensional channel slightly larger than the

dark beads was sufficient to make segmentation very easy. In the two-size experiment several trials were needed in order to choose smaller transparent beads (4 mm) to contrast with the 6 mm dark beads (Hergault et al., 2010).

Distinct segmentation algorithms were used to detect the two types of beads. The problem of tracking particles along a temporal sequence is not straightforward and is known as the point-tracking problem in the literature. Typically, points can be either small object centroids or interest points within larger rigid or unrigid objects. Depending on the application and on the assumptions made regarding point displacement, more or less complex approaches have been proposed (Hwang, 1989; Salari and Sethi, 1990). A particular application is to determine the velocity field of a fluid carrying small particles (Nishino et al., 1989; Fayolle et al., 1996; Udrea et al., 2000). In the studies reported here, Böhm et al. (2006) and Hergault et al. (2010) focused on individual particle motions. Particle velocities differed from those of the surrounding fluid since the particles were coarse and had a higher density than water. Although the use of spherical particles of uniform size made detection easier, the calculation of the trajectories was more difficult since it was not possible to distinguish particles based on their shape. The high frame rate of the camera resulted in a displacement of a particle between two images that was always smaller than the particle diameter. This was essential to achieving a good accuracy with the tracking algorithm as well as to reconstructing trajectories at high resolution (Figure 13.6b).

### 13.3 Channel morphology and flow dynamics

Timelapse imagery of dynamically evolving surfaces are an efficient means for measuring a broad-range of variables characterising channel dynamics and bed evolution at high temporal and spatial resolutions. Timelapse images can be readily compiled into movies showing the continuous evolution of a system. We present some general considerations in acquiring timelapse imagery and present examples on how they have been used in experimental studies of rivers and deltas.

When acquiring timelapse images it is recommended to use cameras that can be computer operated and allow automatic download. Computer operation is important because it helps prevent movement of the camera once it is fixed in place; this is especially important if the camera is mounted in a hard-to-reach location. Having



### 13 The Use of Imagery in Laboratory Experiments 307

images displayed in real time alerts the operator to any problems immediately and prevents a camera stopping mid-experiment because a memory card gets full. Computer operation is particularly useful for operating multiple cameras; images captured simultaneously can be stitched together to capture a larger study area. The software development kit (SDK) that is included with most cameras only allows for one camera to be operated at a time (in other words, a separate computer is required to operate each camera). We are aware of only one commercially available software that permits simultaneous operation of multiple cameras from a single computer: Pine Tree Computing LLC. Many camera SDKs include an option for stitching images and batch processing. In order to successfully stitch images there must be sufficient overlap and the focal length of the images must be the same. It is also important to include stitch points, e.g. clear points that appear in each pair of images to be stitched (these are needed in only one set of images that will be used to automate stitching for a series of images). PTGUI is a commercially available software for stitching images that is independent of a specific camera firmware. Finally, when capturing timelapse images it is recommended the camera be connected to an external power source to prevent it from entering sleep mode between shots or having a battery die mid-run.

Images typically need to be post-processed to rectify lens distortion (curvature) and camera angle (perspective) so that distances and areas are true everywhere in the image. The first step in correcting images is to acquire a calibration image of the study area under the exact conditions that will be used during an experiment. A calibration image consists of a grid composed of parallel and orthogonal horizontal and vertical lines of known dimensions placed parallel to the plane of the experimental surface. The grid can be constructed, drawn onto a board, delineated using stationary markers, etc. (it is recommended to do the calibration before starting an experiment). If the experimental setup (stream-table, camera position, focal length) remains constant the grid can be removed and the same calibration can be used to correct all the images. A new calibration is required whenever any changes are made to the experimental setup. For best results the grid should be as close as possible in size to the field of view of the camera. Once an image is properly corrected the grid-lines should be straight and parallel everywhere in the image and all distances should accurately scale with real-world distances. A computer program can be written to automate image correction for a series of images or widely available commercial image correction software

can be used – Andromeda LensDoc is an example of a commercial Photoshop plug-in that enables setting calibration parameters by simply clicking on different points in the calibration image. The parameters can then be used to batch process a series of images. It is recommended that all images be corrected before stitching.

Common techniques to better visualise naturally transparent flow include adding coloured dye (Winterbottom and Gilvear, 1997; Gran and Paola, 2001; Tal and Paola, 2007) and/or pigments in powder form such as titanium dioxide ( $\text{TiO}_2$ ) to make it opaque (Martin et al., 2009). Adding colour/opacity to the flow makes it much easier to identify both qualitatively and quantitatively from images based on the colour value of each pixel (RGB and HSV; colour value can be read and manipulated using image processing software such as Photoshop and ImageJ or using a program that treats images as matrices such as Matlab). Jpeg image format compresses images and therefore requires less memory than Tiff or Raw, however the latter should be used whenever possible because the colour value of each pixel is preserved.

A constant dye concentration can be used to estimate the flow depth based on colour intensity (Winterbottom and Gilvear, 1997; Gran and Paola, 2001; Tal and Paola, 2007). This technique requires uniform light-coloured sediment; the optimal dye concentration and the variation of colour intensity with flow depth need to be calibrated for every experimental setup. Once a formula relating dye intensity to flow depth has been obtained, flow depth everywhere in the image can be estimated based on the pixel colour value. A simple way to calibrate the flow depth based on colour intensity is to place tilted trays with sediment glued to the bottom and sides and filled with dye water in the camera's field of view. Images should be captured with a camera located directly overhead (normal to the flow). A polariser filter (lens) can be added to the camera in order to reduce glare from the flow. This can be further augmented by placing a polariser sheet in front of any lighting in order to achieve cross-polarisation. The dye-density technique is highly sensitive to variations in lighting which can pose a problem in the case of large experiments. Variations in lighting across the study reach should be identified and multiple calibrations (i.e., trays) should be used to minimise the error. Finally, many dyes photo-degrade (i.e. decay) over time and need to be replenished regularly to maintain a constant concentration. Once again, multiple and continuous calibrations help account for these changes.

## 308 Fluvial Remote Sensing for Science and Management

### 13.3.1 Experimental deltas

The Experimental EarthScape (XES) facility at the St. Anthony Falls Laboratory, University of Minnesota is a research tank designed to study deltaic sedimentation associated with geological controls, e.g., changes in sediment supply, subsidence, and sea-level. Premixed sediment and water are introduced at the upstream end of the flume and flow for a short distance as a fluvial system. At the downstream end of the tank standing water forces sediment to deposit and form a delta. The tank is 3 m wide, 6 m long, and 1.5 m deep. In these experiments deltas self-organise in response to continuously evolving fluvial patterns. Details of these experiments can be found in Kim et al. (2006), Kim and Paola (2007), and Kim and Jerolmack (2008).

Throughout an experiment images of the evolving delta are captured every few seconds using an overhead camera. To better visualise the flow, water is dyed blue and made opaque by adding titanium dioxide. Flow opacity makes it possible to easily distinguish areas with active flow despite the use of two different colours of sediment (in the XES experiments quartz sand is white and crushed coal particles are black). Dye in these experiments was not used for measuring flow depths.

In order to create binary wet-dry images, the contrast between dry and wet areas was first enhanced by creating a greyscale image. For this set of images, differencing the red and blue colour bands produced a greyscale image that clearly highlighted the regions occupied by flow (Figure 13.7). This procedure can be done by, for example, using the 'calculations' option in Adobe Photoshop. Once the greyscale map was obtained, a threshold value was used to convert the image into white (wet) and black (dry) – using the threshold option in Photoshop. The user should be able to identify approximately what flow depth a particular threshold value corresponds to and justify why it is an appropriate cutoff. A series of images can be batch processed once the algorithm has been established.

Analysis of the binary wet and dry images led to the observation that self-organised (autogenic) sediment storage and release are associated with changes in river-planform pattern (Figure 13.8; Kim and Jerolmack, 2008): the experimental deltas stored much of the sediment supplied from the upstream input and showed strong sediment deposition in the deltaic surface when the river pattern was tabular (i.e., sheet flow which corresponds to a large wetted fraction of the bed). In contrast, the delta released sediment stored from the surface through the shoreline to the ocean when the deltaic channels were

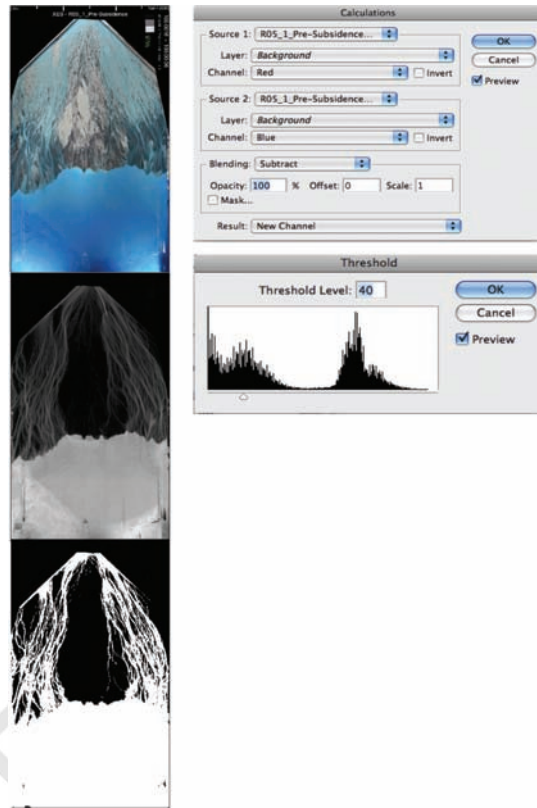


**Figure 13.7** Example of an image analysis from the XES experiment (Kim et al., 2006; Kim and Paola, 2007; Kim and Jerolmack, 2008). The left image is the original colour image, the middle greyscale image is the result of differencing the red and blue colour bands, and the right binary image is based on a threshold value applied to the greyscale image to distinguish between wet (white) and dry (black) pixels.

confined to a narrow path and incised (i.e., channelised flow which corresponds to a small wetted fraction of the bed). The rate of seaward shoreline migration fluctuated as a result of changes in the sediment flux being released from the delta. Autogenic shoreline fluctuation measured from the images corresponded well with the fraction of the fluvial surface that was wet – measured from the binary images.

The analysis of the wetted fraction described above does not reflect the lateral mobility of a channel (i.e., if a channel migrates laterally while maintaining a constant width the wetted fraction remains the same). In order to characterise channel activity (planform pattern change + lateral mobility), Kim and Paola (2007) analysed the wet and dry binary images in a different way. The analysis consisted of accumulating the area of the deltaic surface

## 13 The Use of Imagery in Laboratory Experiments 309

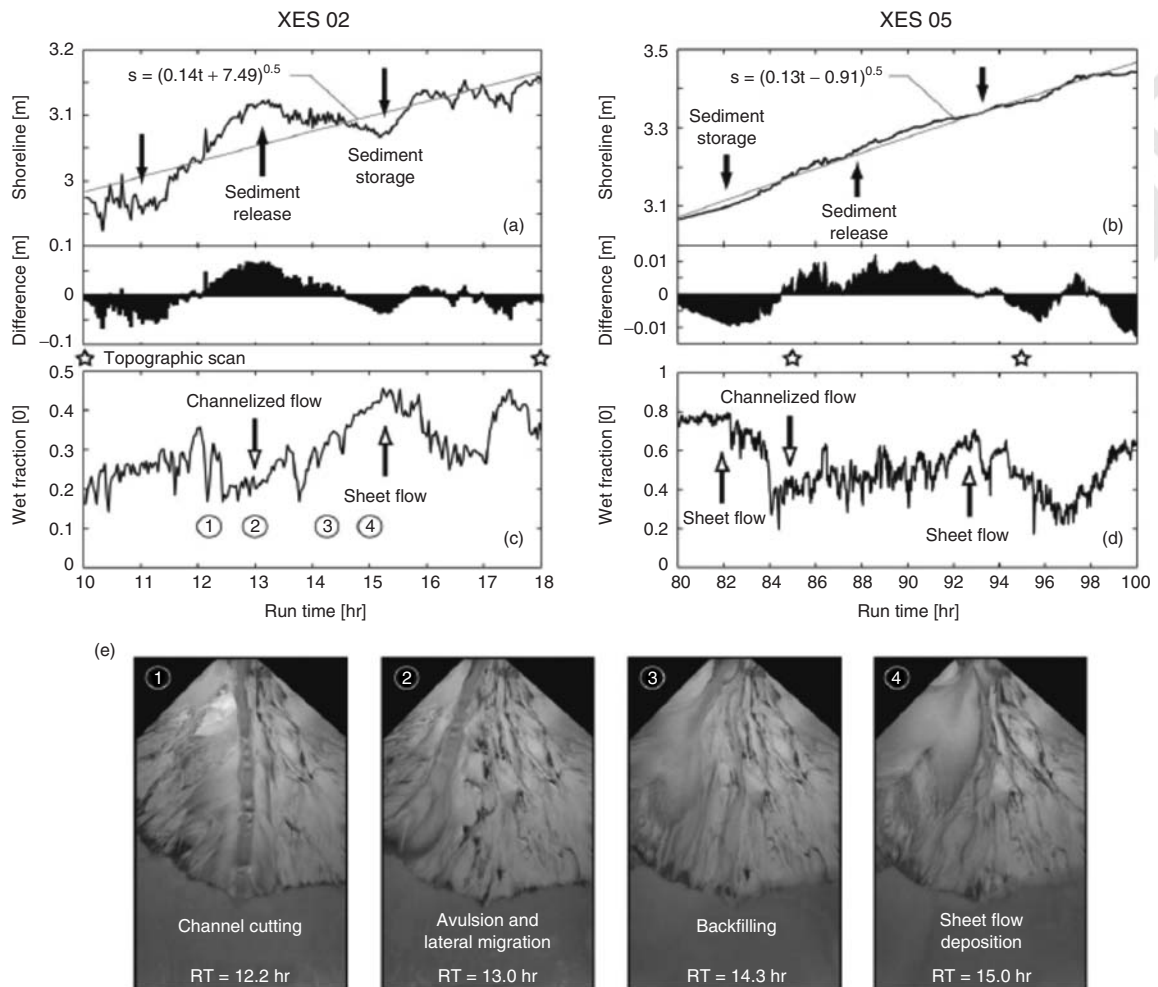


**Figure 13.8** Shoreline and wet-fraction data from the XES experiment (Kim and Jerolmack, 2008). (a and b) Mean shoreline position averaged normal to the mean sediment transport direction and best fit curves. Graphs show shoreline position fluctuation after removal of long-term shoreline regression trend, (c and d) time series of wet fraction showing cyclic changes in fluvial pattern between sheet and channelised flow, (e) representative overhead images showing a cycle of changes in the wet-fraction.

that became wet and the decay (decrease) in the area that remained dry over a set time interval (Figure 13.9). A faster decay represents stronger channel activity and vice-versa. Kim and Paola (2007) used this analysis to compare channel activity during various stages of the experiment that were subject to different external forcing.

### 13.3.2 Experimental river channels with riparian vegetation

In a separate set of experiments at the St. Anthony Falls Laboratory, Tal and Paola (2007, 2010) studied

the dynamic interactions between flow and vegetation. The experiments were designed to investigate whether riparian vegetation could cause a braided channel to evolve to a single-thread channel and were motivated by many field cases in which the encroachment of riparian vegetation was driving a change in planform. The experiments were conducted in a flume 16 m long by 2 m wide with steel walls. Alfalfa sprouts (*Medicago sativa*) were used as the experimental vegetation in the flume. The initial condition for the experiments was steady-state braiding in noncohesive sand under uniform discharge. From here, an experiment consisted of repeated cycles

### 310 Fluvial Remote Sensing for Science and Management

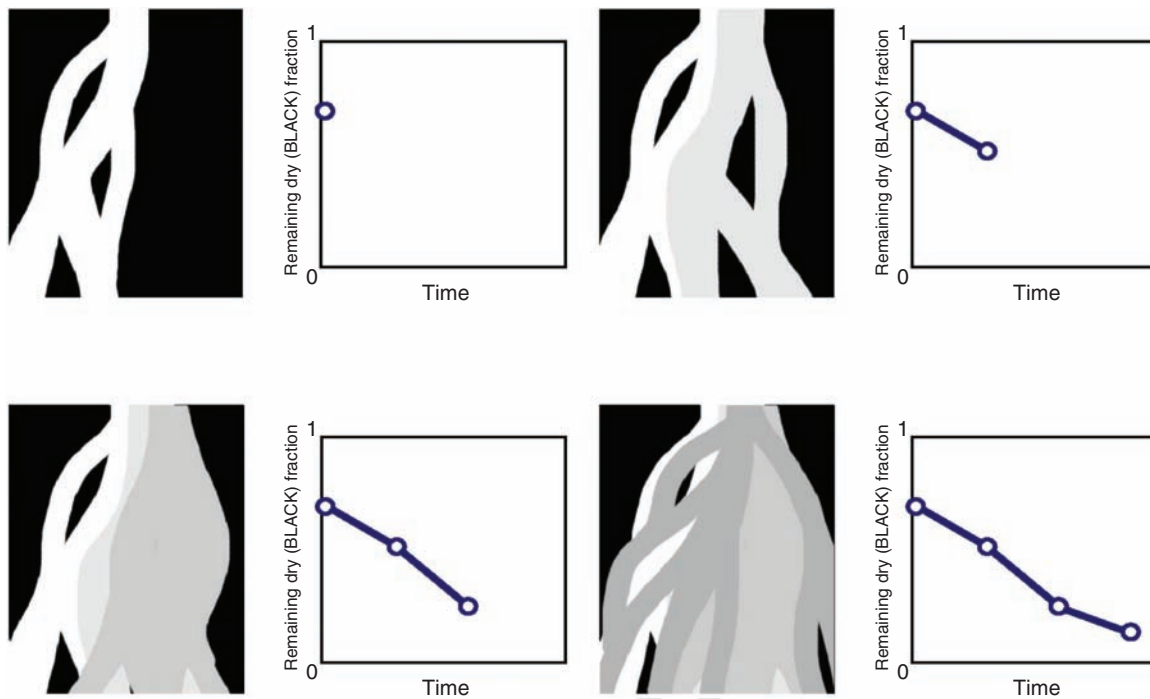


**Figure 13.9** XES image analysis showing the evolution of the deltaic surface over a given time interval. White and grey are respectively the initial wet surface and surfaces that became progressively wet as a result of channel migration. Black is the surface that remained dry. A faster decay in the remaining dry surface corresponds to stronger channel activity (Kim and Paola, 2007).

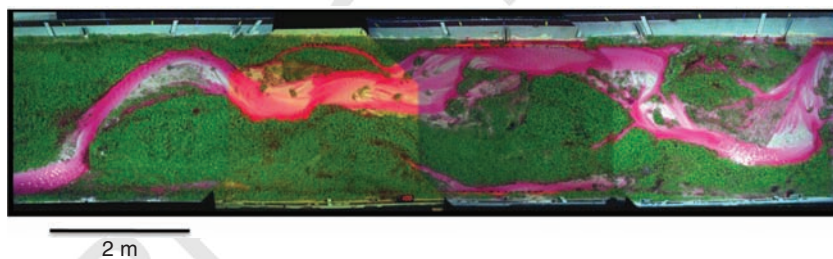


**Figure 13.10** Experimental channel at the St. Anthony Falls Laboratory designed to study the interactions between flow and riparian vegetation (Tal and Paola, 2007; Tal and Paola, 2010). Image is stitched together from four simultaneous time-lapse images. Rhodamine dye is used to colour the flow.

alternating a long duration state of low discharge (3–6 days) during which the channel morphology remained relatively stable and plants grew on emergent river bars and banks, and a short-lived flood (typically 1 hour) with vigorous sediment transport in which physical processes predominated. Vegetation was added to the experiment by dispersing seeds manually over the entire bed at the end of each high flow with the water discharge set to its low value.

Four digital cameras (Olympus C-4000 Zoom) were mounted directly above the flume and equally spaced to capture images of a 10 m long by 2 m wide study reach (Figure 13.10). The images overlapped by  $\sim 0.5$  m so they could be stitched together. The cameras captured images at a resolution of approximately 2 mm/pixel. Each camera had a polarising filter, and polariser sheets were hung underneath the halogen lighting to achieve cross-polarisation and minimise glare from the flow.

### 13 The Use of Imagery in Laboratory Experiments 311

The cameras were controlled remotely using the camera controller software available from Pine Tree Computing LLC and captured simultaneous time-lapse images at intervals of 30-120 seconds during all of the high flows as well as once at the beginning and end of each low flow. Images were post-processed to correct for distortion associated with lens curvature and perspective using the Photoshop Andromeda Lensdoc plug-in. Each set of four simultaneous images was stitched using the commercial software PTGUI to create a single image.

Dye was added to the flow to enhance visualisation as well as to measure flow depth based on colour-intensity. Dyed water was made in batches by mixing 800 litres of water in a large tank with Rhodamine dye at a concentration of 2 ppm. The tank provided the only source of water during the floods in order to maintain a constant concentration of dye. Flow was recirculated with a pump. This procedure was used for all experiments that had a one-hour flood duration. In experiment with a four-hour high flow photodegradation of the dye did not permit flow recirculation. Instead, dye and water were fed in at a constant rate at the inlet. Tilted trays with sand glued to the bottom and sides were filled with dye water and used to calibrate depth variation with colour intensity (Figure 13.11). The calibration trays were placed at least once during each flood in the field of view of each of the four cameras and left permanently on the bed wherever possible without disturbing the flow dynamics. The minimum calibration error associated with the calibration trays was, on average,  $\pm 1$  mm. In order to minimise calibration errors depth was estimated for each camera separately using the tray for that image only, and as close in time as possible to the time the image was captured.

Wetted widths and channel migration rates were measured from flow maps created from time-lapse images captured at 5 minute intervals during the floods. Colour images were first converted into binary images in which all the flow had a value of 1 (white) and all dry areas (sand + veg) had a value of 0 (black; Figure 13.12a and 13.12b). A threshold hue value of 0.8 and a saturation value of 0.3 were used to distinguish between wet and dry and the process was automated using Matlab. Data were extracted along transects normal to the images and spaced 0.05 m apart over the entire study reach (total of 226 transects). A cross-stream width of 0.06 m was set as a threshold for a group of wet pixels to be considered a channel. Wetted widths were calculated as the sum of wet pixels averaged over a downstream distance of 0.3 m (6 transects). Channel migration rates were calculated by summing the area (in pixels) that was converted from dry to wet between consecutive pairs of images and dividing this area by the total length of the image. Changes over 5-min intervals encompassed both gradual lateral migration as well as abrupt ( $<5$  min) channel shifts from one location to another.

Analysis of flow maps for these experiments were used to measure how wetted width, number of active channels (braiding index), migration rates, and channel sinuosity evolved as the braided channels transitioned to single-thread channels (Tal and Paola, 2010). Similar to the analysis described above by Kim and Paola (2007) and using a technique developed by Wickert (2007), flow maps were used to measure the timescale for loss of pattern information, i.e. the time required for the entire bed to get reworked once by the flow. The number of pixels representing flow in the first image of a series that

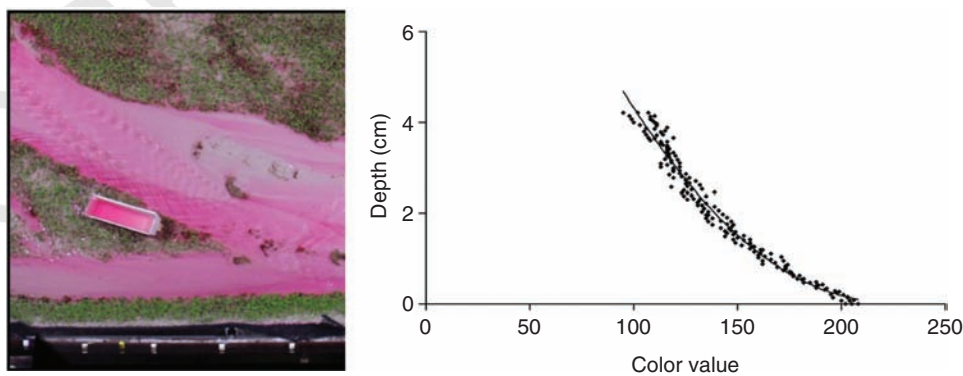
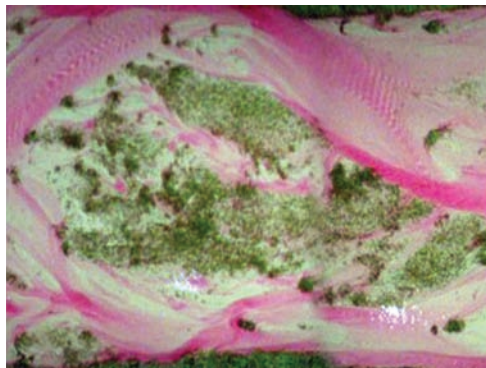


**Figure 13.11** Flow with Rhodamine dye, calibration tray, and curve showing depth variation with colour intensity (Tal and Paola, 2007; Tal and Paola, 2010).

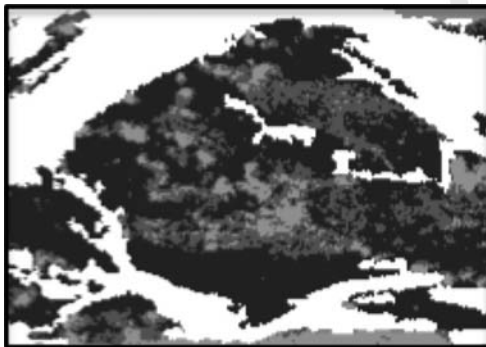
### 312 Fluvial Remote Sensing for Science and Management



(a)



(b)



(c)

**Figure 13.12** Example of part of a classified image (1 m × 1 m) (a) original image, (b) binary image, wet is white, black is dry, (c) area that was black in b classified into bare-sparse vegetation (black), dense vegetation (dark gray), very dense vegetation (light grey; Tal, 2008).

continued to contain flow at each subsequent time step was recorded (pixels that became dry, i.e., abandoned or vegetated and then wet again were not counted). The analysis demonstrated that vegetation slows the reworking time of the bed compared to unvegetated braiding. This reduction was attributed to a combination of slower erosion rates due to increased bank strength and the limited ability of opportunistic creation of new channels in areas not occupied by the flow due to the deterrence effect of plants (Tal and Paola, 2010).

Transition matrices were used to study feedbacks between flow and vegetation establishment. To do this, pixels representing dry riverbed in the binary flow maps were further classified into three additional classes representing different stages of vegetation cover (plant age and density; Figure 13.12c). The three main stages of vegetation cover were first visually identified in the images, then their distinct colour signature was measured (Figure 13.13). The colour value of the plants at different stages represented a combination of both plant age and density: dense clumps of young vegetation could have the same colour value as sparse patches of mature plants. Using the classified images transition matrices were computed for pairs of images at 5-minute intervals during all of the high flows as well as between high and low flows. The transition matrices shed light on important feedbacks between flow and vegetation and the role of a fluctuating discharge. A key effect of the plants was to colonise abandoned (dry) areas during low flow and to deter the high flow from reoccupying these areas during the next flood, leading to progressive reinforcement of the low flow wetted width (Tal and Paola, 2010). The analysis also demonstrated that vegetation colonisation was a highly self-reinforcing process: areas where plants survived early provided a more stable surface for new plants to establish. As new vegetation established it further stabilised these areas and increased their chances of surviving subsequent floods (Figure 13.14). As a result, vegetated islands expanded through time and merged with other islands to form larger islands. This continuous process of accretion and amalgamation of islands eventually resulted in the formation of a permanently vegetated floodplain (Figure 13.10; Tal, 2008).

#### 13.4 Bed topography and flow depth

Approaches to measuring bed topography range from simple manual point-gauges to sophisticated laser and ultrasonic scanners mounted on automated carriages

## 13 The Use of Imagery in Laboratory Experiments 313

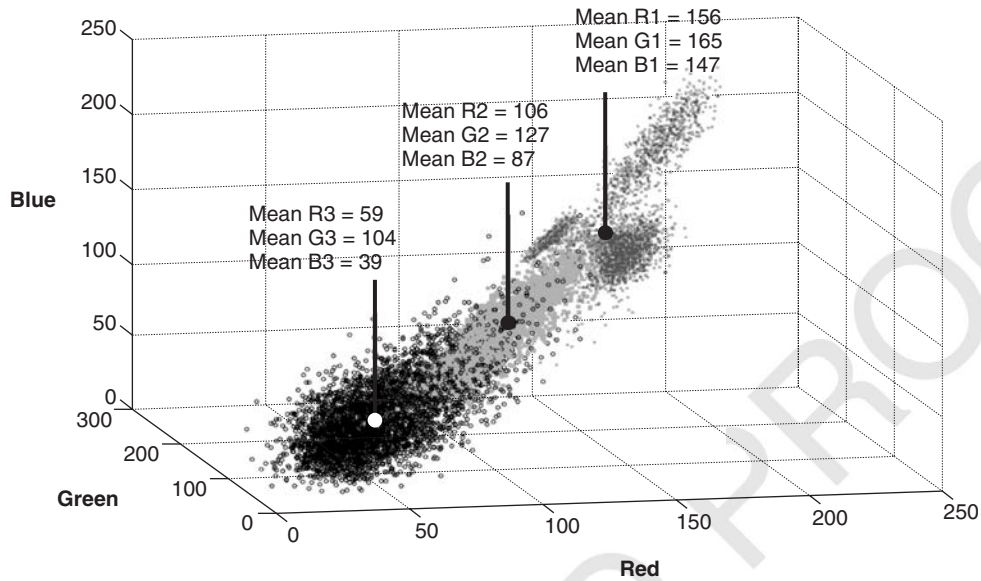


**Figure 13.13** Pixels from vegetation samples plotted in colour space. Each colour/symbol represents the class that the sample corresponded to in the visual classification. The plot shows that the classes that were discerned visually do indeed fall into distinct classes based on their colour value (Tal, 2008; Tal and Paola, *in prep.*).

(e.g., Kim and Paola, 2007; Hoyal and Sheets, 2009). Another common technique consists of projecting single or multiple laser line(s) onto the bed and photographing it with a camera mounted at an oblique angle; vertical displacements of the line are calibrated to real-world changes in elevation (Figure 13.15; Leaf et al., 1993; Hasbargen and Paola, 2000; Lague et al., 2003). These point-by-point or line-by-line techniques are discontinuous in space and some can be very time-consuming, requiring long pauses in the experiment to perform each scan. Digital photogrammetry is one method that provides a way of measuring topography over a continuous surface (Chandler et al., 2001; Lane et al., 2001; Turowski et al., 2006). However, all these methods require a separate technique and setup to measure flow depths. For example, combinations of laser measurements and dye-density (discussed above) have been used to simultaneously measure both flow depth and bed topography (e.g. Huang et al., 2010).

Here we describe an optical method known as moiré for acquiring measurements of both bed topography and flow depth in laboratory experiments (Sansoni et al., 1999). The moiré projection method is part of a general family of techniques that use the projection of structured light to measure relief (Patorski, 1993) and enables image-based non-contact measurements over a continuous surface at very high spatial and temporal

resolutions. The moiré method has been successfully applied in metrology studies (Chiang, 1979), industrial inspection (Sansoni, 2000), human body mapping for medical diagnosis (Halioua, 1989; Kozłowski, 1997) and art inspection (Bremand, 2007).

A moiré method is based on projecting a fringe pattern (also known as a grating or grid) on the bed and analysing the deformation of the pattern caused by the topography with respect to a fringe pattern projected on a reference plane (i.e., a flat bed; Figure 13.16). The height of the object (i.e., topography) is encoded in the phase difference between the two patterns which is retrieved through a Fourier transform or phase shifting algorithms (Figure 13.17). While the mathematics behind the method is rather complex, the good news is the methodology is relatively easy to implement and user-friendly commercial software that perform the calculations automatically are available. For details about the theory and mathematical operations readers should refer to Sansoni et al. (1999), Pouliquen and Forterre (2002), and Limare et al. (2011). Here we present only the basics behind the method, considerations for implementing it, and an example from a study of braided channels.

The simplest way to implement a moiré method consists of capturing an image (or series of images) of a single

## 314 Fluvial Remote Sensing for Science and Management

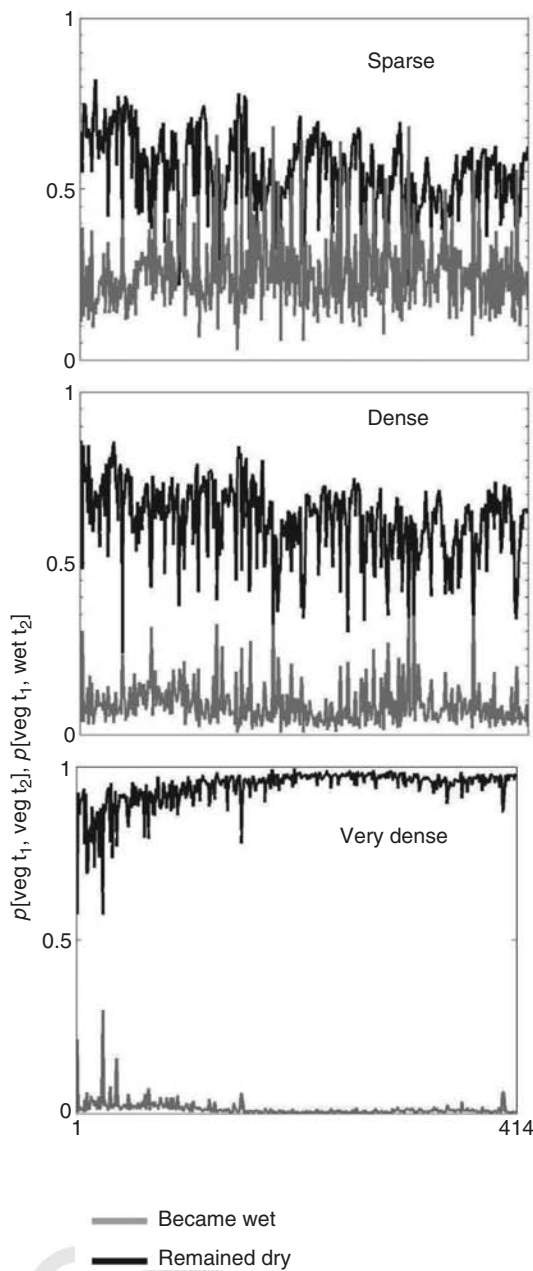


**Figure 13.14** Probability by vegetation class of an area that was vegetated at  $t_1$  to get eroded (become wet) at  $t_2$  versus the probability that it will remain dry at  $t_2$ . Probabilities were calculated between images captured at 5-minute intervals during all of the high flows (Tal, 2008).

grid projected onto an evolving surface (using a video or more simply an overhead projector) and analysing the deformation of the grid with respect to the same grid projected on a flat plane (e.g., a smooth bed at the beginning of an experiment; Figure 13.16). The projection angle of the grid should be sufficiently small such that bed topography induces a significant deformation. Photos of the plane are recorded with a digital camera positioned vertically above the bed. The spectrum of grid patterns of the reference image and an image containing topography are analysed using the Fourier transform (Figure 13.17). The local shift of the grid lines (i.e., phase-difference) between the deformed pattern in the presence of topography and the reference pattern is contained in the width of the peak in the spectrum analysis and is proportional to the local thickness of the bed (i.e. topography). The phase difference is converted to bed elevation based on a calibration that relates the measured phase shift to a known change in elevation (Figure 13.17).

The simplified version of the moiré method described above has been used in laboratory physical experiments to study granular flows (Pouliquen and Forterre, 2002), incision dynamics of subaqueous channels (Lancien, 2005), and micro-scale braided rivers (Metivier and Meunier, 2003). The costs involved with this type of moiré setup include a digital camera, a computer, and a video-projector (or even less expensive – an overhead projector), the sum of which is substantially lower than of a laser scanner but without compromising precision. Data acquisition and processing are relatively fast so measurements can be made in quasi-real time and data processing can be automated.

A more elaborate but more precise implementation of the moiré method uses a procedure known as phase shifting to calculate the phase and robust phase unwrapping combined with grey coding to assess the geometric parameters (details in Limare et al., 2011). A more sophisticated phase-to-height conversion is based on a calibration using a plane tilted at a known incline rather than a stationary object (Figure 13.18). Rather than a single-grid projection, a series of different grid patterns are projected automatically in succession. Images are captured with a CDD camera connected to the same computer generating the grid patterns. The number of projected images can be varied making it possible to switch between high resolution and fast acquisition time according to the requirements of the experiment.

Regardless which moiré method is used, certain general requirements must be fulfilled in order to obtain the best raw images as input data. First, the grid projection must



## 13 The Use of Imagery in Laboratory Experiments 315

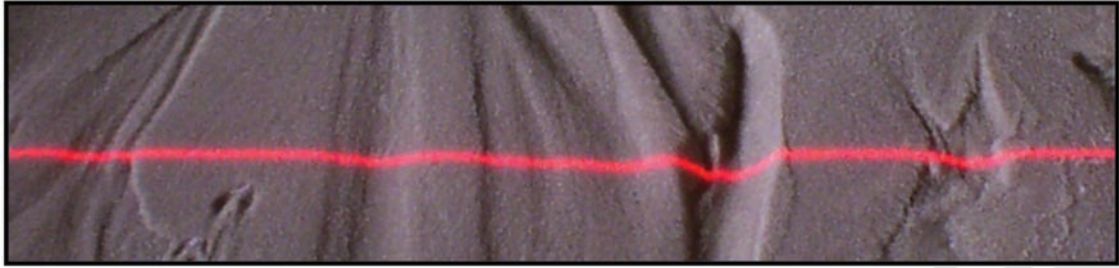


**Figure 13.15** Example of a laser line ( $\sim 0.4$  m) projected onto a sediment bed and photographed with a camera mounted at an oblique angle (Tal, 2008).

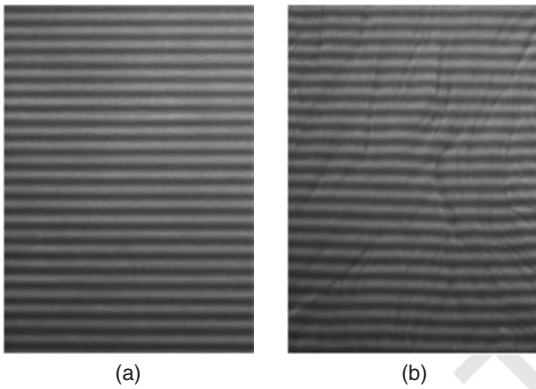


**Figure 13.16** (a) Reference image (1 m long  $\times$  0.5 m wide) of a fringe pattern projected onto a flat bed and (b) a deformed fringe pattern due to bed topography formed by braided channels (Limare et al., 2011).

have a constant frequency across the experimental surface. If the projector has a significant incidence angle (either to project over a larger area or to reduce glare if water is present), it may be necessary to compensate for this angle when creating the grid to ensure a constant frequency across the entire plane. In general, the moiré method works well for light coloured, relatively uniform diffusive substrate. As in the other imaging methods discussed, glare should be reduced using polariser filters and sheets. Images should be corrected for lens and perspective distortion before any analysis.

A key advantage to the moiré method is the ability to estimate flow depths based on the refraction of light at the air/water interface. Bed topography reconstructed by any method based on grid deformation when water is present on the bed will be distorted relative to bed topography measured on a dry surface. This distortion can be used to estimate flow depth from images acquired with and without flow. Assuming the flow is locally

uniform (free surface parallel to the bed surface), light from the projector will bend normal to the surface and will produce a bright spot when hitting the surface. From the point of view of the camera, the bright spot is observed in the direction corresponding to the angle  $i_c$  with respect to the normal (Figure 13.19):

$$\frac{\sin i_p}{\sin r_p} = \frac{\sin i_c}{\sin r_c} = n_{\text{water}} \quad (13.4)$$

where  $n_{\text{water}}$  is the refractive index of water. The difference in elevation between the apparent location of the bright spot ( $h$ ) and the true depth ( $H$ ) is obtained by trigonometry:

$$H = \frac{\tan i_p + \tan i_c}{\tan r_p + \tan r_c} h \quad (13.5)$$

The difference between topographies obtained with and without flow will give a distorted bathymetry that is always shallower than the true bathymetry and a correction factor for the incidence angle needs to be applied. Incidence angles can be calculated for any point using simple trigonometry:  $i_p, i_c = f(i, j)$ . In the case of parallel projection and observation beams, the relation between true and distorted bathymetry has a simplified form:  $H = n_{\text{water}} h$ .

A moiré projection method was used to study the evolution of microscale braided channels (Figure 13.20; Limare et al., 2011). Experiments similar to the one here are described in detail in Metivier and Meunier, (2003). The experiments were conducted at the IGP experimental geomorphology laboratory in a stream-table that was 1.5 m long and 0.75 m wide with a fully adjustable bed. The initial slope of the bed was approximately 0.05. The sediment in these experiments was composed of glass beads with a  $D_{50}$  of 250 micron and a density of  $2500 \text{ kg/m}^3$ . The initial condition for each experiment was a flat bed with a straight channel (0.01 m deep and 0.02 m wide) carved down the middle. The flow was laminar and a

## 316 Fluvial Remote Sensing for Science and Management

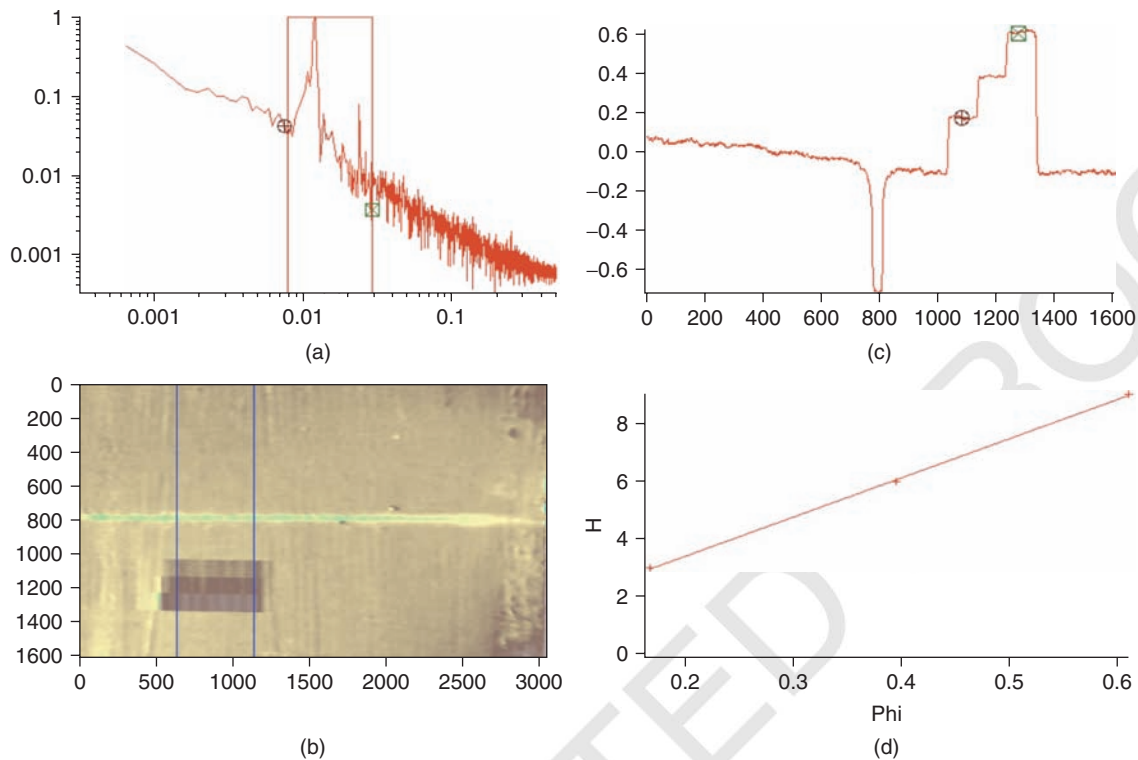


**Figure 13.17** Steps involved in a moiré method analysis: (a) spectrum of the reference image obtained using the Fourier transform, (b) an image of the bed topography reconstructed from the phase shift between the reference image and an image with a straight channel carved into the bed and an object of known dimensions (consisting of three stairs), (c) a profile from top to bottom of one of the transects in b, (d) phase-to-height calibration based on the known heights of the three stairs.

fully braided morphology spontaneously developed and reached steady state (sediment input equaled sediment output) after a few hours. Sediment and water were supplied continuously at the upstream end of the flume at a constant rate. Flow discharge was around  $2.5 \times 10^{-5} \text{ m}^3/\text{s}$  and sediment discharge was approximately  $8 \times 10^{-8} \text{ m}^3/\text{s}$ . Glare caused by flow was reduced by using two cross axis polarisers placed in front of the projector and the camera respectively. A moiré method was implemented to measure bed topography and flow depth using a commercial software package called Light3D – developed at the Laboratory of Solid State Mechanics, University of Poitiers, France (Breque et al., 2004). The program uses phase shifting to calculate the phase and robust phase unwrapping combined with grey coding to assess the geometric parameters. The user can choose the number of phase-shifted patterns to be projected (3, 8, 16 or 32) and phase unwrapping can be performed with or without 8 grey code images. For the results shown here the

phase field was calculated with 8 phase-shifted images and robust unwrapping using a series of 8 grey code images. The computer generated patterns were projected from a Sanyo PLV-Z5 video-projector. A black and white  $\mu$  eye Stemmer Imaging CCD camera ( $1280 \times 1024$  pixels) was used for image acquisition. Prior to each experiment a calibration procedure was carried out using a flat, white, highly diffusive board that could be tilted following the procedures outlined by the software. In addition to the phase-to-height conversion, the software uses the calibration to automatically calculate all the required geometrical parameters which can be difficult to measure accurately manually (Figure 13.18).

Over the course of an experiment bed topography and water depth were measured every 10 minutes in the following manner: ‘wet’ bed topography was measured with the flow on, the flow was turned off, ‘dry’ bed topography was measured after the flow was off for 1 minute (the time required for the bed to be uniformly drained). Water



### 318 Fluvial Remote Sensing for Science and Management

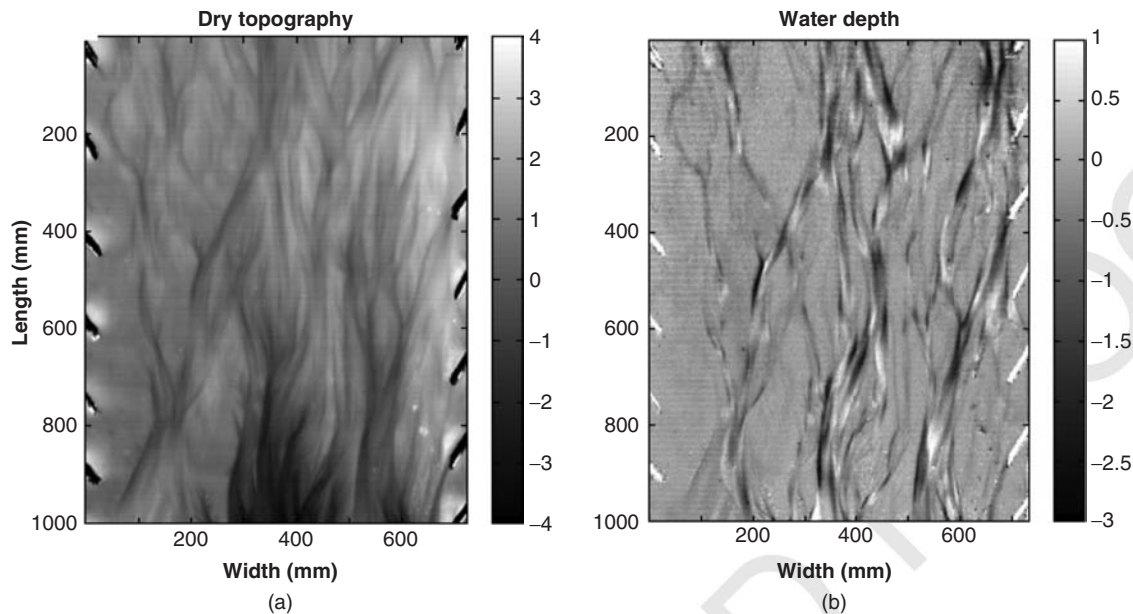


**Figure 13.20** Results of a moiré projection method, (a) bed topography obtained with flow turned off, zero represents the original flat reference bed (b) flow depths obtained by subtracting images with and without flow (Limare et al., 2011). Flow increases in the negative direction. Zero represents dry bed. Positive flow depths represent noise that was later removed.

the experimental setup. The equipment required typically involves at least one digital camera or video recorder and computer to operate the camera remotely and download photos automatically. The type of camera that should be used depends on the method, e.g., basic digital camera for acquiring timelapse images (multiple cameras or a wide-angle can be used for large experiments), high-speed video recorder for PTV, and CDD camera for a moiré method. The latter also requires a video-projector. Camera's usually include software enabling control of only one camera at a time per computer, however commercial software is available for operating multiple cameras simultaneously from a single computer. Most of the difficult work involved in imaging techniques in conjunction with laboratory experiments is in the initial setup, assuming the setup remains constant thereafter. Once all equipment is placed in the optimum position (e.g., height and distance of the camera and projector), the optimal conditions have been established (e.g. lighting, dye concentration, colour of the sediment), and all necessary calibrations have been made (e.g., stitch points, image rectification), data acquisition is relatively fast and simple with minimal disruption to the experiment. While many image processing techniques are based on complicated equations and algorithms, user-friendly software are available to guide

users who do not wish to develop their own programs from scratch. Equipped with such software, excellent results can be achieved with only a basic understanding of the technique and adequate trial and error. Likewise, software is available to batch-process operations such as image rectification, cropping, stitching, colour thresholds, etc. for a large series of images.

#### Acknowledgements

We are grateful to Maarten Kleinhans and Richard Hardy for reviewing this chapter and for providing helpful comments.

#### References

- Adrian, R.J. 2005. Twenty years of particle image velocimetry, *Exp Fluids* 39: 159–169.
- Ancy, C., Bigillon, F., Frey, P., Lanier, J., and Ducret, R. 2002. Saltating motion of a bead in a rapid water stream. *Phys Rev E* 66 (3): 036306.
- Ancy, C., Bigillon, F., Frey, P., and Ducret, R. 2003. Rolling motion of a bead in a rapid water stream, *Phys Rev E* 67 (1): 011303.

## 13 The Use of Imagery in Laboratory Experiments 319

- Ancey, C., Böhm, T., Jodeau, M., and Frey, P. 2006. Statistical description of sediment transport experiments. *Phys Rev E* 74 (1): 011302
- Ancey, C., Davison, A.C., Böhm, T., Jodeau, M., and Frey, P. 2008. Entrainment and motion of coarse particles in a shallow water stream down a steep slope, *J Fluid Mech* 595: 83–114.
- Ashmore, P.E. 1991b. How do gravel bed rivers braid?, *Canadian Journal of Earth Science* 28: 326–341.
- Bigillon, F., Frey, P., Ducottet, C., Vierin, N., Ancey, C., Richard, D., and Lanier, J. 1999. Développement d'une technique d'analyse d'images pour la caractérisation du transport solide par charriage, *FLUVISU* 99, pp. 275–280, Toulouse, France.
- Böhm, T., Ancey, C., Frey, P., Reboud, J.L., and Ducottet, C. 2004. Fluctuations of the solid discharge of gravity-driven particle flows in a turbulent stream, *Phys Rev E* 69(6): 061307.
- Böhm, T., Frey, P., Ducottet, C., Ancey, C., Jodeau, M., and Reboud, J.L. 2006. Two-dimensional motion of a set of particles in a free surface flow with image processing, *Exp Fluids* 41: 1–11.
- Brémard, F., Doumalin, P., Dupré, J., Hesser, F., and Valle, V. 2007. Optical techniques for relief study of analysis of Mona Lisa's wooden support, Proceedings of the 13<sup>th</sup> International Conference on Experimental Mechanics, Gdoutos, Greece.
- Breque, C., Dupré, J.C., and Brémard, F. 2004. Calibration of a system of projection moiré for relief measuring: biomechanical applications, *Optics and Lasers in Engineering* 41: 241–260.
- Buscombe, D. and Masselink, G. 2009. Grain-size information from the statistical properties of digital images of sediment, *Sedimentology* 56: 421–438.
- Buscombe, D., Rubin, D.M., and Warrick, J.A. 2010. A universal approximation of grain size from images of noncohesive sediment, *Journal of Geophysical Research* 115: F02015.
- Canny, J. 1986. A computational approach to edge detection, *IEEE Transactions on Pattern Analysis and Machine Intelligence* 8: 679–698.
- Capart, H., Liu, H.H., Van Crombrughe, X., and Young, D.L. 1997. Digital imaging characterization of the kinematics of water-sediment interaction, *Water Air and Soil Pollution* 99: 173–177.
- Capart, H., Young, D.L., and Zech, Y. 2002. Voronoï imaging methods for the measurement of granular flows, *Exp Fluids* 32: 121–135.
- Chandler, J.H., Shiono, K., Rameshwaren, P., and Lane, S.N. 2001. Measuring flume surfaces for hydraulics research using a Kodak DCS460, *The Photogrammetric Record* 17: 39–61.
- Chiang, F. 1979. Moiré methods of strain analysis, *Experimental Mechanics* 19(8): 290–308.
- Diplas, P., Dancy, C.L., Celik, A.O., Valyrakis, M., Greer, K., and Akar, T. 2008. The role of impulse on the initiation of particle movement under turbulent flow conditions, *Science* 322 (5902): 717–720.
- Ducottet, C. 1994. Application of wavelet transforms to the processing of tomographic and holographic images of fluid flow, PhD Dissertation, University of Saint Etienne, France.
- Fayolle, J., Ducottet, C., Fournel, T., and Schon, J.P. 1996. Motion characterization of unrigid objects by detecting and tracking feature points, *IEEE International Conference on Image Processing*, Lausanne, Switzerland, pp. 803–806.
- Frey, P., Ducottet, C., and Jay, J. 2003. Fluctuations of bed load solid discharge and grainsize distribution on steep slopes with image analysis, *Exp Fluids* 35: 589–597.
- Gomez, B. and Church, M. 1989. An assessment of bed load sediment transport formulae for gravel bed rivers, *Water Resources Research*, 25(6): 1161–1186.
- Graham, D.J., Reid, I., and Rice, S.P. 2005. Automated sizing of coarse-grained sediments: Image- processing procedures, *Mathematical Geology* 37: 1–28.
- Gran, K. and Paola, C. 2001. Riparian vegetation controls on braided stream dynamics, *Water Resources Research*, 37(12): 3275–3283.
- Halioua, M. and Liu, H.-C. 1989. Optical three-dimensional sensing by phase measuring profilometry, *Optics and Lasers in Engineering* 11: 185–215.
- Hasbargen, L.E. and Paola, C. 2000. Landscape instability in an experimental drainage basin, *Geology* 28 (12): 1067–1070.
- Hergault, V., Frey, P., Métivier, F., Barat, C., Ducottet, C., Böhm, T., and Ancey, C. 2010. Image processing for the study of bedload transport of two-size spherical particles in a supercritical flow, *Experiments in Fluids* 49(5): 1095–1107.
- Hooke, R.L. 1975. Distribution of sediment transport and shear stress in a meander bend, *Journal of Geology* 83: 543–565.
- Hoyal, D.C. and Sheets, B.A. 2009. Morphodynamic evolution of experimental cohesive deltas, *Journal of Geophysical Research* 114: F02009.
- Hu, C.H. and Hui, Y.J. 1996. Bed-load transport. 1. Mechanical characteristics. *J. Hydraul. Eng.* 122(5): 245–254.
- Huang, M., Huang, A., and Capart, H. 2010. Joint mapping of bed elevation and flow depth in microscale morphodynamics experiments, *Experiments in Fluids* 49(5): 1121–1134.
- Hwang, V.S.S. 1989. Tracking feature points in time-varying images using an opportunistic selection approach, *Pattern Recognition* 22: 247–256.
- Ikeda, S., Parker, G., and Kimura, Y. 1988. Stable width and depth of straight gravel rivers with heterogeneous bed materials, *Water Resources Research* 24: 713–722.
- Jernot, J.P., Coster, M., and Chermant, J.L. 1982. Model to describe the elastic modulus of sintered materials, *Phys. Stat. Sol. (a)*. 72(1): 325–332.
- Kim, W. and Jerolmack, D.J. 2008. The pulse of calm fan deltas, *Journal of Geology* 116 (4): 315–330.
- Kim, W. and Paola, C. 2007. Long-period cyclic sedimentation with constant tectonic forcing in an experimental relay ramp, *Geology* 35 (4): 331–334.
- Kim, W., Paola, C., Swenson, J.B., and Voller, V.R. 2006. Shoreline response to autogenic processes of sediment storage and release in the fluvial system, *J. Geophys. Res.* 111: F04013.
- Kozłowski, J. and Giovanni, S. 1997. New modified phase locked loop method for fringe pattern demodulation, *Opt. Eng.* 36: 2025–2030.

### 320 Fluvial Remote Sensing for Science and Management

- Lague, D., Crave, A., and Davy, P. 2003. Laboratory experiments simulating the geomorphic response to tectonic uplift, *J. Geophys. Res.* 108 (B1): 2008.
- Lajeunesse, E., Malverti, L., and Charru, F. 2010. Bed load transport in turbulent flow at the grain scale: Experiments and modeling, *J. Geophys. Res.* 115: F04001.
- Lancien, P., Metivier, F., Lajeunesse, E., and Cacas, M. 2005. Incision dynamics and shear stress measurements in submarine channels experiments, in *River, Coastal and Estuarine Morphodynamics*, Parker and Garcia (eds), Taylor and Francis Group, London.
- Lane, S.N., Chandler, J.H., and Porfiri, K. 2001. Monitoring river channel and flume surfaces with digital photogrammetry, *J. Hydraul. Eng.* 127: 871.
- Leaf, R.B., Wilson, B.N., and Hansen, B.J. 1993. Field instrumentation for measuring soil topography, ASAE Summer Meeting, Spokane, Washington, Pap. 932111, 19 pp., Am. Soci. of Agric. Eng., St. Joseph, Michigan.
- Lee, H.Y., Chen, Y.H., You, J.Y., and Lin, Y.T. 2000. Investigations of continuous bed load saltating process. *J. Hydraul. Eng.* 126: 691–700.
- Limare, A., M.Tal, Reitz, M., Lajeunesse, E., and Metivier, F. 2011. Optical method for measuring bed topography and flow depth in an experimental flume, *Solid Earth* 2: 143–154.
- Martin, J., Sheets, B., Paola, C., and Hoyal, D. 2009. Influence of steady base-level rise on channel mobility, shoreline migration, and scaling properties of a cohesive experimental delta, *Journal of Geophysical Research* 114: F03017.
- Métivier, F. and Meunier, P. 2003. Input and output mass flux correlations in an experimental braided stream: Implications on the dynamics of bed load transport, *Journal of Hydrology* 271: 22–38.
- Meyer-Peter, E. and Müller, R. 1948. Formulas for Bed-Load Transport, Proceedings 2nd Congress, International Association of Hydraulic Research, Stockholm, pp. 39–64.
- Nezu, L. and Azuma, R. 2004. Turbulence characteristics and interaction between particles and fluid in particle-laden open channel flows, *J. Hydraul. Eng.* 130: 988–1001.
- Niño, Y., Garcia, M., and Ayala, L. 1994. Gravel Saltation. 1. Experiments, *Water Resour. Res.* 30: 1907–1914.
- Nishino, K., Kasagi, N., and Hirata, M. 1989. Three-dimensional particle tracking velocimetry based on automated digital image processing, *J. Fluids Eng.* 111(4): 384–392.
- Okamoto, K., Hassan, Y.A., and Schmidl, W.D. 1995. New Tracking Algorithm for Particle Image Velocimetry. *Exp Fluids* 19: 342–347.
- Papanicolaou, A.N., Diplas, P., Balakrishnan, M., and Dancy, C.L. 1999. Computer vision technique for tracking bed load movement, *Journal of Computing in Civil Engineering* 13: 71–79.
- Parker, G., Dhamotharan, S., and Stefan, H. 1982. Model experiments on mobile, paved gravel bed streams, *Water Resources Research*, 18 (5): 1395–1408.
- Patorski, K. 1993. *Handbook of the moiré fringe technique*, Elsevier, New York, 431 p.
- Pilotti, M., Menduni, G., and Castelli, E. 1997. Monitoring the inception of sediment transport by image processing techniques, *Exp Fluids* 23: 202–208.
- Pouliquen, O. and Forterre, Y. 2002. Friction law for dense granular flows: application to the motion of a mass down a rough inclined plane, *Journal of Fluid Mechanics* 453: 133–151.
- Radice, A., Malavasi, S., and Ballio, F. 2006. Solid transport measurements through image processing, *Exp Fluids* 41: 721–734.
- Recking, A., Frey, P., Paquier, A., and Belleudy, P. 2009. An experimental investigation of mechanisms responsible for bedload sheet production and migration, *J. Geophys. Res.* 114: F03010.
- Rubin, D.M. 2004. A simple autocorrelation algorithm for determining grain size from digital images of sediment, *Journal of Sedimentary Research*, 74 (1).
- Salari, V. and Sethi, I.K. 1990. Feature point correspondence in the presence of occlusion. *IEEE Transactions on Pattern Analysis and Machine Intelligence* 12: 87–91.
- Sansoni, G., Carocci, M., and Rodella, R. 1999. 3D vision based on the combination of gray code and phase shift light projection: analysis and compensation of the systematic errors, *Appl. Opt.* 31: 6565–6573.
- Sansoni, G., Carocci, M., and Rodella, R. 2000. Calibration and performance evaluation of a 3D imaging sensor based on the projection of structured light, *IEEE Trans. Instrum. Meas.*, 49: 628–635.
- Sapozhnikov, V.B. and Fofoula-Georgiou, E. 1997. Experimental evidence of dynamic scaling and indications of self-organized criticality in braided rivers, 33 (8): 1983–1991.
- Seal, R. and Paola, C. 1995. Observations of downstream fining on the North Fork Toutle river near Mount St. Helens, Washington, *Water Resources Research* 31: 1409–1419.
- Sechet, P. and Le Guennec, B. 1999. The role of near wall turbulent structures on sediment transport. *Water Resources Research* 33: 3646–3656.
- Spinewine, B., Capart, H., Larcher, M., and Zech, Y. 2003. Three-dimensional Voronoï imaging methods for the measurement of near-wall particulate flows, *Exp Fluids* 34: 227–241.
- Tal, M. 2008. Interactions between vegetation and braiding leading to the formation of single-thread channels, PhD Thesis, University of Minnesota.
- Tal, M. and Paola, C. 2007. Dynamic single-thread channels maintained by the interactions of flow and vegetation, *Geology* 35: 347–350.
- Tal, M. and Paola, C. 2010. Effects of vegetation on channel morphodynamics: results and insights from laboratory experiments, *Earth Surface Processes and Landforms* 35(9): 1014–1028.
- Turowski, J., Lague, D., Crave, A., and Hovius, N. 2006. Experimental channel response to tectonic uplift, *Journal of Geophysical Research* 111: F03008.
- Udrea, D., Bryanston-Cross, P., Querzoli, G., and Moroni, M. 2000. *Particle tracking velocimetry techniques in Fluid mechanics and its application*, Kluwer Academic, pp. 279–304.

### 13 The Use of Imagery in Laboratory Experiments 321

- Wickert, A. 2007. Measuring channel mobility through the analysis of area-based change in analog experiments, with insights into alluvial environments, Bachelors thesis, Massachusetts Institute of Technology.
- Wilcock, P.R. 2001. The flow, the bed, and the transport: Interaction in flume and field, in *Gravel-Bed Rivers*, V., edited by M. Mosley, N. Z. Hydrol. Soc., Wellington, pp. 183–219.
- Wilcock, P.R. and Crowe, J.C. 2003. Surface-based transport model for mixed-size sediment, *Journal of Hydraulic Engineering* 129(2): 120–128.
- Wilcock, P.R. and McArdell, B.W. 1993. Surface-based fractional transport rates: mobilization thresholds and partial transport of a sand-gravel sediment, *Water Resources Research* 29(4): 1297–1312.
- Winterbottom, S.J and Gilvear, D.J. 1997. Quantification of channel bed morphology in gravel-bed rivers using airborne multispectral imagery and aerial photography, *Regulated Rivers: Research & Management* 13: 489–499.
- Zimmermann, A.E., Church, M., and Hassan, M.A. 2008. Video-based gravel transport measurements with a flume mounted light table, *Earth Surface Processes and Landforms* 33: 2285–2296.

UNCORRECTED PROOFS



**Queries in Chapter 13**

Q1. Figure 13.1 is not cited in the text.

UNCORRECTED PROOFS